

Feature Space Perturbation: A Panacea to Enhanced Transferability Estimation

Prafful Kumar Khoba¹ Zijian Wang² Chetan Arora³ Mahsa Baktashmotlagh²

¹UQ–IITD Research Academy, New Delhi, India

²The University of Queensland, Brisbane, Australia

³Indian Institute of Technology Delhi, New Delhi, India

qiz228274@iitd.ac.in, zijian.wang@uq.edu.au, chetan@cse.iitd.ac.in, m.baktashmotlagh@uq.edu.au

Abstract

Leveraging a transferability estimation metric facilitates the non-trivial challenge of selecting the optimal model for the downstream task from a pool of pre-trained models. Most existing metrics primarily focus on identifying the statistical relationship between feature embeddings and the corresponding labels within the target dataset, but overlook crucial aspect of model robustness. This oversight may limit their effectiveness in accurately ranking pre-trained models. To address this limitation, we introduce a feature perturbation method that enhances the transferability estimation process by systematically altering the feature space. Our method includes a Spread operation that increases intra-class variability, adding complexity within classes, and an Attract operation that minimizes the distances between different classes, thereby blurring the class boundaries. Through extensive experimentation, we demonstrate the efficacy of our feature perturbation method in providing a more precise and robust estimation of model transferability. Notably, the existing LogMe method exhibited a significant improvement, showing a 28.84% increase in performance after applying our feature perturbation method. The implementation is available at https://github.com/prafful-kumar/enhancing_TE.git

To address this issue, researchers have proposed various metrics [24, 28, 30, 34, 39, 40, 44, 45] based on the distinctive properties of the pre-trained model, known as the transferability estimation metric. The core idea behind many of these metrics is to establish a statistical relationship between the feature embedding of pre-trained models and the labels of the samples, thereby generating a transferability score for each model. Based on the score, these metrics aim to predict the actual rank of these models on the target dataset, with the goal of achieving a high correlation between the predicted rank and the actual rank, as shown in Fig. 1(a). However, while these metrics effectively measure adaptability, they often overlook how models handle disruptions in the structure of the embeddings, which is crucial for assessing their robustness. To fill this gap, we propose a novel approach that perturbs both the intra-class (through the spread operation) and inter-class (through the attract operation) structures of the embeddings. By introducing this targeted perturbation, we aim to provide a more comprehensive and realistic assessment of a model’s resilience and adaptability. This method not only improves the accuracy of transferability estimations but also ensures that the selected models are genuinely capable of performing reliably in diverse and dynamic environments.

To illustrate how robustness to perturbations impacts transferability estimation, consider a toy example depicted in Fig. 1. The figure visually illustrates how embeddings respond to perturbations and its impact on model transferability. Initially, the embeddings display clear inter-class separation and compact intra-class configurations Fig. 1(a), typical of supervised models’ structured embeddings. After our feature perturbation method is applied Fig. 1(b), these embeddings show expanded intra-class distributions and reduced inter-class separations, highlighting how perturbations disrupt the standard embedding structure. As traditional metrics rely adaptability of the features, they tend to produce lower transferability scores post-perturbation for all the models. Yet, the degree of score reduction varies significantly among the models. This is evident on the x-axis

1. Introduction

Transfer learning enables the application of knowledge acquired from one task to enhance performance on another with only minimal additional training, typically through fine-tuning [46]. At the core of this approach is the challenge of transferability estimation, which aims to predict how well the pre-trained models adapt when applied to new, target datasets without fine-tuning. However, the main challenge lies in determining the most appropriate model for a specific task without individually fine-tuning each candidate model, which can be a resource-intensive and time-consuming task, especially for large target datasets.

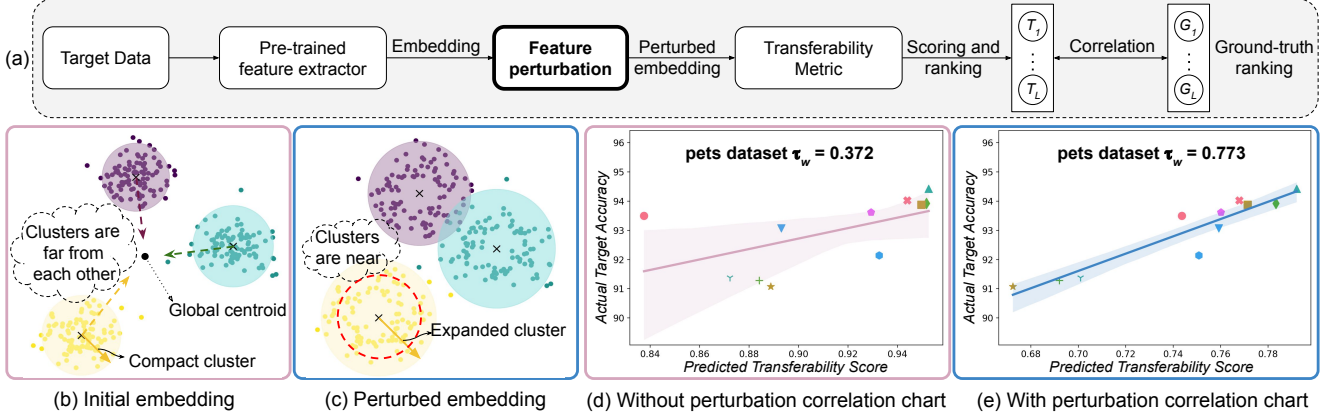


Figure 1. Illustration of our feature perturbation method for transferability estimation. (a) provides a flowchart outlining the process of enhancing transferability estimation, with bold elements representing our perturbation steps. The remaining part of the flowchart illustrates the process traditionally employed in existing transferability estimation work. (b) shows initial embeddings with significant inter-class separation and compact intra-class clustering, typical of supervised models. (c) displays embeddings after our feature perturbation. (d) and (e) present actual correlation charts and weighted Kendall correlation coefficient τ_w on the pets dataset. Correlation chart depicts the predicted rankings versus actual rankings before and after perturbations, where each symbol in these charts represents a model. The shift from lower to higher correlation values highlights the improved accuracy of model rankings after applying our perturbation method.

of the correlation chart for the pets dataset in Fig. 1(d,e), as referenced from the results section 4.2. For instance, if one model’s score drops drastically compared to others, it indicates a lower robustness to perturbations. This substantial decrease suggests that the model’s embeddings are overly sensitive to changes, potentially undermining its performance when applied to new datasets. This leads to a more accurate relative ranking of these models.

While most of the prior works focus on estimating the transferability of models under the vanilla fine-tuning schema, we argue that it may not be sufficient to address a broader use case. Recent literature [18, 21] highlights that while vanilla fine-tuning can achieve higher in-distribution (ID) test accuracy, it sacrifices the out-of-distribution (OOD) robustness compared with alternative fine-tuning strategy (*i.e.*, linear probing). The trade-off between ID and OOD test accuracy urges transferability estimation metrics to consider a wider range of fine-tuning schemes. Therefore, in this work, we assess the transferability estimation metric for three distinct fine-tuning strategies: *vanilla fine-tuning*, which updates all model parameters; *last block fine-tuning (LBFT)*, which updates only the parameters of the last block and final linear layer; and *linear fine-tuning (LFT)*, which focuses on updating the last fully connected layer. In summary, our contribution is threefold:

- Our feature perturbation method effectively perturbs the feature embedding spaces of pre-trained supervised models, significantly improving the rank estimation of these pre-trained models by transferability estimation metric. This approach led to a notable 28.84% performance boost in the LogMe [44] method.

- Our findings highlight that existing metrics are primarily effective for vanilla fine-tuning, pointing out the necessity for more adaptable solutions for diverse fine-tuning techniques. Our feature perturbation method significantly enhances transferability estimation across key fine-tuning strategies, specifically vanilla and LBFT. Its effectiveness across these strategies and compatibility with all current transferability estimation metrics underscores its broad applicability and versatility.
- Unlike supervised models, self-supervised models do not rely on labeled data and are particularly sensitive to disruptions in their geometric embedding structures. Therefore, we avoid applying our class-based perturbation strategy to these models. Instead, we have developed a Linear Discriminant Analysis [2] (LDA)-based metric, specifically tailored for self-supervised models, that significantly outperforms traditional baselines across all fine-tuning variants.

2. Related Work

Prior work can be categorized into label-based method and source-embedding based method. Log Expected Empirical Predictor (LEEP) [28] and Negative Conditional Entropy (NCE) [39] are two transferability estimation metrics that rely on information from both the source and target label sets. Passing target data through a pre-trained model’s feature extractor yields target embeddings for source-embedding methods. These methods include \mathcal{N} LEEP [24], LogMe [44], SFDA [34], NCTI [40], and GBC [30].

\mathcal{N} LEEP [24] is build to remove the drawbacks of LEEP, i.e., it does not uses source head. It utilizes Principal Component Analysis (PCA) [41] to reduce the dimensionality of the data, followed by fitting a Gaussian Mixture Model (GMM) [32] to the target data embedding. LogMe [44] assesses model transferability by modeling each target label as a linear model with Gaussian noise using maximum evidence to evaluate how well pre-trained model features fit target labels. GBC [30] metric evaluates how much classes in the target data’s embedding space overlap; a higher GBC value indicates greater overlap. SFDA, presented in [34], is a transferability metric which employs Fisher Discriminant Analysis (FDA) [27] and introduces ConfMix. FDA works by finding a linear data transformation that maximizes the separation between classes using within-class scatter and between-class scatter followed by applying ConfMix, a mechanism to generate challenging negative samples. NCTI [40] metric quantifies the gap between a model’s embedding and the ideal neural collapse embedding.

Li et al. [23] proposed Potential Energy Decline (PED), a physics-inspired method modeling interactive forces to capture model adaptability during fine-tuning. Menta et al. [26] improved transferability estimation by selecting informative subsets of the target dataset using pre-trained model representations. However, existing methods overlook robustness in transferability estimation. Our study addresses this gap by introducing a framework that integrates adaptability and robustness for more reliable transferability metrics.

3. Methodology

In this section, we outline the problem definition, our proposed method, transferability estimation metrics, and the evaluation criteria for model selection. For the sake of simplicity, we use image classification as our primary task throughout the paper.

3.1. Preliminaries

Problem definition: Let $\mathcal{T} = \{X, Y\}$ represent the target dataset, and $\{\phi_l\}_{l=1}^L$ denote L the pre-trained feature-extractors, with l being the index. Using transferability estimation, given by \mathcal{M} , our goal is to rank these pre-trained models based on their performance on a given target dataset. We assess the transferability of each pre-trained model using a specific metric \mathcal{M} that produces a numerical score, denoted as T_l . Essentially, a higher score for T_l implies that the model ϕ_l is more likely to perform effectively on the given target dataset.

Ground truth: To establish a reliable basis for comparing pre-trained models, a process of fine-tuning each model on the target dataset is conducted, accompanied by a thorough exploration of different hyperparameters (i.e., learning rate and weight decay). Test accuracy obtained from this fine-

tuning is then utilized as a ‘ground truth’ for the ranking of these models. The fine-tuning performance of each model is notated as $\{G_l\}_{l=1}^L$, serving as a benchmark for evaluating the model ranking by transferability estimation metric.

3.2. Proposed Approach

Source-embedding based transferability estimation metrics [24, 30, 34, 40, 44] leverage features extracted from pre-trained models to estimate their adaptability to a downstream task. Our proposed feature perturbation method systematically tests the robustness of model embeddings by applying controlled perturbations. Recognizing that the embedding structure varies with the feature extractor and the target dataset, our method avoids a one-size-fits-all perturbation. Instead, it dynamically adjusts the perturbation magnitude to preserve the meaningful structure of embeddings. We achieve this through two operations called spread and attract (SA), which are described below:

Spread operation: One of the desirable properties of features in supervised learning is high intra-class compactness [3]. The Spread operation deliberately perturbs the internal structure of each class by increasing the intra-class variance, effectively decreasing intra-class compactness. This perturbation pushes examples that were previously near the centroid—and thus easier to classify—further away, increasing their variability and making them more challenging to classify correctly. Specifically, for every class, we compute the centroid of the class C_u as given by Eq. 2 and displace each data point uniformly away from its centroid, given by:

$$\hat{\mathbf{X}}_{\text{spread},u} = \hat{\mathbf{X}}_u + \left(\frac{\hat{\mathbf{X}}_u - C_u}{\|\hat{\mathbf{X}}_u - C_u\|_2} \right) \quad (1)$$

$$C_u = \frac{1}{n_u} \sum_{i=1}^{n_u} \hat{\mathbf{X}}_{u,i} \quad (2)$$

where $\hat{\mathbf{X}}_{\text{spread},u}$ represents the feature embeddings for class u after the spread operation, C_u is the centroid of class u , $\hat{\mathbf{X}}_u$ is the reduced-dimensionality embedding of class u obtained after applying PCA on the extracted feature embeddings, and n_u is the number of samples in class u .

Attract operation: Another desirable property of features in supervised learning is high inter-class separability [3]. Supervised models for classification tasks generally learn clear boundaries between classes in feature space. The attract operation aims to diminish this separation by adjusting class embeddings according to the distances between their centroids and variance, thereby perturbing the feature space to create closer inter-class proximities. This operation tests the resilience of the model’s embeddings in scenarios where class boundaries are intentionally blurred. The attract operation is formulated as:

$$\hat{\mathbf{X}}_{\text{attract}_u} = \hat{\mathbf{X}}_{\text{spread}_u} + \alpha \cdot \mathbf{Disp}_{uv} \quad (3)$$

where, $\hat{\mathbf{X}}_{\text{attract}_u}$ is the feature embedding of the class u after applying the attract method to $\hat{\mathbf{X}}_{\text{spread}_u}$, α is a hyper-parameter that modulates the magnitude of the displacement towards the other class centroids, and \mathbf{Disp}_{uv} is:

$$\mathbf{Disp}_{uv} = \sum_{v \neq u} \left(\frac{\mathbf{D}_{uv}}{\|\mathbf{D}_{uv}\|_2} \right) \cdot (\|\mathbf{D}_{uv}\|_2 - (\sigma \cdot R_u + \sigma \cdot R_v))$$

$$R_u = \sqrt{\frac{1}{n_u} \sum_{i=1}^{n_u} \|\mathbf{X}_{u,i} - \mathbf{C}_u\|^2} \quad (4)$$

Here, $\mathbf{D}_{uv} = \mathbf{C}_u - \mathbf{C}_v$ is the distance vector between the centroids \mathbf{C} of two different classes, u and v . σ is a hyper-parameter that adjusts the sensitivity of the displacement to the variability within class embeddings, as measured by R_u and R_v . Attract operation ensures that the perturbations are proportionate to the natural variability within and between the classes. This approach helps to preserve the meaningful structure of the embeddings while testing their resilience against perturbations.

Algorithm 1: SA algorithm

Input: Target dataset $\mathcal{T} = \{X, Y\}$, pre-trained models $\{\phi_l\}_{l=1}^L$, hyper-parameters σ, α , transferability metric \mathcal{M}

Output: Transferability scores T_l for each model

```

1 for  $l = 1$  to  $L$  do
2    $\hat{X} \leftarrow \text{PCA}(\phi_l(X))$ 
3   for each class  $k$  in  $Y$  do
4      $C_k \leftarrow \text{Compute centroid of } \hat{X}_k$ 
5     for each point  $X_{k,i}$  in class  $k$  do
6        $D_{k,i} \leftarrow \frac{X_{k,i} - C_k}{\|X_{k,i} - C_k\|_2}$ 
7        $X_{\text{spread}_{k,i}} \leftarrow X_{k,i} + D_{k,i} \text{ // Spread}$ 
8   for each class pair  $(u, v)$  do
9      $D_{uv} \leftarrow C_u - C_v$ 
10     $R_u \leftarrow \|\text{Std}(\hat{X}_u)\|_2, R_v \leftarrow \|\text{Std}(\hat{X}_v)\|_2$ 
11    for each  $X_{\text{spread}_{u,i}}$  in class  $u$  do
12       $\text{Disp}_{uv,i} \leftarrow \sum_{v \neq u} \frac{D_{uv}}{\|D_{uv}\|_2} \cdot (\|D_{uv}\|_2 - (\sigma \cdot R_u + \sigma \cdot R_v))$ 
13       $X_{\text{attract}_{u,i}} \leftarrow X_{\text{spread}_{u,i}} + \alpha \cdot \text{Disp}_{uv,i}$ 
14      // Attract
15     $T_l \leftarrow \mathcal{M}(X_{\text{attract}}, Y)$ 
16 Rank models based on  $T_l$ .
```

The importance of controlled perturbation: Fig. 2(b) demonstrates an optimal level of perturbation that preserves

the necessary balance and structural integrity required for accurate transferability estimation. Conversely, Fig. 2(c) shows how suboptimal perturbation settings can result in excessive alterations, complicating the feature space and hindering transferability assessment. These examples underline the crucial role of carefully calibrated perturbations in ensuring reliable model evaluations.

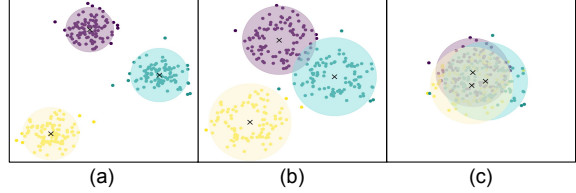


Figure 2. Demonstrating the importance of controlled perturbation in feature space manipulation, using a toy example. (a) Represents the initial target embedding. (b) depict an appropriate amount of feature perturbation, while (c) demonstrate excessive levels of feature perturbation.

3.3. Overall Objective

Our feature perturbation method systematically alters the feature embedding representation for target dataset $\mathcal{T} = \{X, Y\}$ using $\{\phi_l\}_{l=1}^L$ feature extractor of the pre-trained model. We then compute the transferability score for each model $\{T_l\}_{l=1}^L$ using the metric \mathcal{M} , which assesses the perturbed embeddings $\hat{\mathbf{X}}_{\text{attract}}$ against the target labels \mathbf{Y} , as shown in the equation below.

$$T_l = \mathcal{M}(\hat{\mathbf{X}}_{\text{attract}}, \mathbf{Y}) \quad (5)$$

For each feature extractor ϕ_l , the algorithm extracts feature embeddings and applies PCA to get a reduced-dimensionality representation, \hat{X} . This step is crucial for managing computational complexity and focusing on the most informative features of the embeddings. The algorithm for our perturbation method is given in Algorithm 1.

4. Experiments

This section is organized into five distinct parts to evaluate the proposed feature perturbation method. Section 4.1 outlines the experimental setup; Section 4.2 presents the results; Section 4.3 covers the ablation study; Section 4.4 examines hyper-parameter sensitivity; Section 4.5 analyzes time complexity; and section 4.6 presents the result on self-supervised architectures.

4.1. Experiment Setup

Datasets. Our study utilizes a diverse collection of datasets commonly used in transferability estimation research [34]. The collection contains fine-grained object classification dataset (i.e., Oxford-102 Flowers [29], Food-101 [4], Stanford Cars [19], FGVC Aircraft [25], Oxford-IIIT Pets [31]),

Table 1. Performance comparison (average weighted Kendall τ_w) between original and enhanced frameworks for vanilla fine-tuning on supervised models. For a pair of rows, the original metric is presented first followed by the corresponding enhanced metric. Best results are highlighted in bold. Our framework consistently outperforms the original framework across all metrics.

Method	Aircraft	Caltech-101	Cars	CIFAR10	CIFAR100	DTD	Flowers	Food-101	Pets	Sun	VOC	Average
\mathcal{N} /LEEP [24]	-0.449	0.769	0.602	0.783	0.717	0.796	0.295	0.581	0.511	0.944	0.710	0.569
SA + \mathcal{N} /LEEP	0.236	0.626	0.763	0.910	0.843	0.836	0.435	0.657	0.829	0.790	0.828	0.704
LogME [44]	0.439	0.497	0.605	0.852	0.725	0.700	0.147	0.385	0.411	0.511	0.695	0.542
SA + LogME	0.442	0.655	0.603	0.924	0.855	0.784	0.743	0.665	0.447	0.788	0.782	0.698
GBC [30]	0.423	0.213	0.617	0.735	0.664	0.703	0.214	0.548	0.514	0.271	0.743	0.513
SA + GBC	-0.110	0.473	0.591	0.928	0.789	0.713	0.510	0.711	0.651	0.803	0.787	0.622
SFDA [34]	0.614	0.615	0.574	0.949	0.866	0.575	0.492	0.815	0.545	0.558	0.671	0.661
SA + SFDA	0.414	0.598	0.801	0.901	0.908	0.816	0.736	0.681	0.865	0.790	0.816	0.756
NCTI [40]	0.496	0.492	0.662	0.843	0.879	0.616	0.541	0.773	0.867	0.756	0.741	0.697
SA + NCTI	0.872	0.483	0.805	0.843	0.878	0.776	0.714	0.619	0.856	0.790	0.800	0.767

Table 2. Performance comparison (average weighted Kendall τ_w) between original and enhanced frameworks for LBFT on supervised models. For a pair of rows, the original metric is presented first followed by the corresponding enhanced metric. The optimal outcomes are emphasized in bold. Our framework consistently exceeds the performance of the original framework across all metrics.

Method	Aircraft	Caltech-101	Cars	CIFAR10	CIFAR100	DTD	Flowers	Food-101	Pets	Sun	VOC	Average
\mathcal{N} /LEEP [24]	-0.415	0.370	0.159	0.732	0.803	0.593	-0.035	0.667	0.505	0.691	0.512	0.417
SA + \mathcal{N} /LEEP	0.305	0.735	0.848	0.757	0.853	0.629	0.020	0.742	0.529	0.641	0.777	0.621
LogME [44]	0.386	0.577	0.453	0.789	0.640	0.715	0.286	0.690	0.192	0.627	0.222	0.507
SA + LogME	0.223	0.260	0.633	0.739	0.831	0.548	0.458	0.783	0.233	0.622	0.707	0.548
GBC [30]	0.676	0.076	0.476	0.631	0.751	0.612	0.176	0.790	0.349	0.395	0.210	0.467
SA + GBC	-0.164	0.541	0.626	0.656	0.767	0.650	0.133	0.749	0.149	0.641	0.777	0.502
SFDA [34]	0.395	0.432	0.324	0.702	0.671	0.585	0.414	0.553	0.372	0.393	0.142	0.453
SA + SFDA	0.174	0.754	0.864	0.765	0.775	0.768	0.361	0.708	0.698	0.610	0.764	0.658
NCTI [40]	0.366	0.441	0.447	0.728	0.760	0.395	0.150	0.637	0.766	0.848	0.388	0.539
SA + NCTI	0.620	0.652	0.942	0.739	0.789	0.568	0.415	0.730	0.685	0.641	0.792	0.688

coarse-grained object classification dataset (*i.e.*, Caltech-101 [12], Cifar-10 [20], Cifar-100 [20], Voc2007 [11]), one scene classification dataset (*i.e.*, Sun397 [43]), and one texture classification dataset (*i.e.*, DTD [10]). These datasets provide a broad spectrum of challenges under various scenarios.

4.2. Experimental Results

Overview. To evaluate the performance of transferability estimation metrics, we initiate the model pool by following the existing work [34]. Specifically, the model pool consists of 11 ImageNet pre-trained architectures, including InceptionV1 [35], InceptionV3 [36], ResNet50 [15], ResNet101 [15], ResNet152 [15], DenseNet121 [16], DenseNet169 [16], DenseNet201 [16], MobileNetV2 [33], and NASNet-A Mobile [37].

Ground truth and correlation measurement. We follow the grid search described in [34], which selects the learning rates from $\{10^{-1}, 10^{-2}, 10^{-3}, 10^{-4}\}$ and weight decay parameters from $\{10^{-6}, 10^{-5}, 10^{-4}, 10^{-3}\}$. To ensure the robustness and reliability of our evaluation, we execute the code using five distinct seeds for each experiment and then take the average of target accuracy. For evaluation, we use weighted Kendall [17] correlation coefficient τ_w because

it assigns weights to the concordant and discordant pairs based on their positions in the ranking; A high positive τ_w value indicates a strong correlation, while a negative value implies an inverse correlation.

Performance comparison on vanilla fine-tuning. In this part, we consider vanilla fine-tuning, which updates all parameters during the training process. We report the experimental results in Table 1. As can be seen from the table, SA feature perturbation method demonstrates notable improvements in transferability estimation across all previous metrics. In particular, our proposed method achieves a relative improvement of 23.86 % on \mathcal{N} /LEEP, 28.84% on LogMe, 21.27% on GBC, 14.46% on SFDA, 10.04% on NCTI, and with the LogMe metric benefiting the most from this approach. The table reports an average improvement of 19.69% on previous SOTA transferability estimation methods, indicating the effectiveness of our approach.

Meanwhile, our perturbation strategy demonstrates variably beneficial outcomes in a few datasets. For example, on Aircraft, our methods can only improve three out of five baseline metrics. We argue that embedding structure for a few datasets contains class overlap causing mixed improvements for various metrics. To understand the intrinsic difference of these datasets, we randomly sample three classes

Table 3. Comparison (average weighted Kendall τ_w) between original and enhanced frameworks for LFT on supervised models. In each pair of rows, the original metric is listed first, followed by the corresponding enhanced metric. The superior results are emphasized in bold.

Method	Aircraft	Caltech-101	Cars	CIFAR10	CIFAR100	DTD	Flowers	Food-101	Pets	Sun	VOC	Average
\mathcal{N} LEEP [24]	0.422	0.685	0.747	0.558	0.509	0.790	0.378	0.512	0.717	0.746	0.698	0.615
SA + \mathcal{N} LEEP	0.615	0.760	0.328	0.831	0.705	0.635	0.285	0.615	0.677	0.244	0.824	0.592
LogME [44]	0.127	0.247	0.144	0.490	0.359	0.721	0.170	0.229	-0.128	0.198	0.470	0.275
SA + LogME	-0.129	0.363	0.073	0.907	0.883	0.634	0.465	0.625	0.178	0.262	0.689	0.450
GBC [30]	-0.048	0.266	0.124	0.359	0.373	0.440	0.121	0.330	0.209	0.228	0.531	0.267
SA + GBC	-0.308	0.628	0.044	0.935	0.818	0.758	0.304	0.694	0.096	0.244	0.824	0.457
SFDA [34]	0.320	0.475	0.508	0.611	0.558	0.380	0.429	0.709	0.119	0.574	0.432	0.465
SA + SFDA	0.585	0.934	0.381	0.882	0.905	0.855	0.307	0.684	0.751	0.251	0.812	0.667
NCTI [40]	0.656	0.775	0.572	0.627	0.636	0.526	0.589	0.675	0.431	0.521	0.667	0.607
SA + NCTI	0.182	0.833	0.381	0.907	0.840	0.738	0.423	0.635	0.706	0.244	0.839	0.611

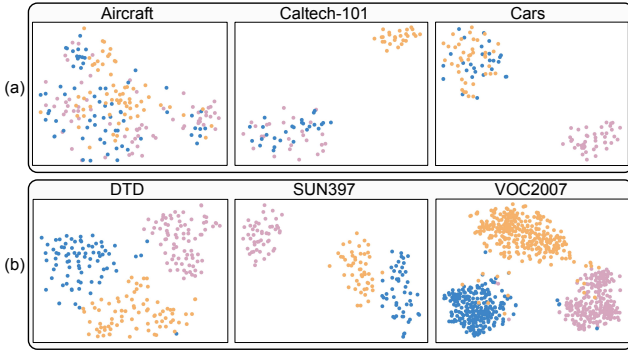


Figure 3. Visualization of ResNet50 target embeddings before feature perturbation (best viewed in color): (a) Represents datasets exhibiting mixed improvement for various metrics, shown in Table 1. The presence of class overlap in (a) contributes to the varied performance across metrics. In contrast, (b) depicts datasets demonstrating consistent improvement across all other evaluated metrics, facilitated by well-separated embeddings. This distinction underscores the role of embedding structure in the estimation.

and visualize the feature distribution of (a) variably beneficial datasets and (b) consistent beneficial datasets in Fig. 3. One can see from the figure that the class-conditional feature distribution largely overlaps with each other. A similar pattern can be seen in other datasets like Caltech-101 and Cars. Given the well-separated feature embeddings in set (b), our perturbation method has a more pronounced effect in enhancing transferability estimation. This improvement is evident in the column corresponding to the dataset in Table 1.

Performance comparison on fine-tuning variants. In this work, we study the performance of transferability estimation metrics under two alternative fine-tuning strategies, namely LBFT and LFT. LBFT updates the last convolutional block and the final linear layer of the network, and LFT only updates the final linear layer with all other parameters frozen in the training process. More details can be found in the supplementary material.

Table 2 shows the ranking performance of the models

trained under the LBFT strategy. Although the order of rank of the estimation metrics remains largely consistent between vanilla fine-tuning and LBFT, the overall ranking correlation drops from 0.59 to 0.47. This suggests that previous metrics could be vulnerable when applied to LBFT. Following SA feature perturbation, there is a substantial performance boost of 27.47% for LBFT, proving the effectiveness of our feature perturbation method in enhancing accurate transferability estimation specifically for LBFT scenarios.

Compared to vanilla fine-tuning, LFT can be deployed faster, with improved performance on out-of-distribution (OOD) test samples. The ranking performance under the LFT strategy is shown in Table 3. While a strategy like LFT does not change the structure of the feature space during training, our approach can still achieve a predominantly beneficial result. SA feature perturbation strategy improves three out of five comparison metrics, scoring 0.142 weighted Kendall τ_w increase. The results reflect that our approach is suitable to adopt in the LFT use case.

4.3. Ablation Study

To validate the effectiveness of each component in the proposed methods, we conduct an ablation study of the Spread and Attract operation on four different baseline transferability estimation metrics (*i.e.*, NCTI, SFDA, LogMe, and GBC). We show the experimental results in Fig. 4. From the figure, we can observe that the application of both the Spread and Attract operations brings improvement in ranking correlations. On average, the Spread operation yields a 10.57% improvement, while the Attract operation provides a 14.57% improvement. The Attract operation’s superior performance can be attributed to its sophisticated approach that accounts for both the intra-class coherence and the inter-class separations before perturbation. Specifically, as defined in Eq 3, the Attract operation applies changes to the embeddings after considering the distance between class centroids (\mathbf{D}_{uv}) and the L2 norm of standard deviations within the classes (R_u and R_v). This allows for perturbations that are informed by a holistic view

Table 4. Performance comparison (average weighted Kendall τ_w) for vanilla fine-tuning on self-supervised models. In each column, the best results are highlighted in bold. Remarkably, LDA achieves the highest overall average weighted Kendall’s τ_w score.

Method	Aircraft	Caltech-101	Cars	CIFAR10	CIFAR100	DTD	Flowers	Food-101	Pets	Sun397	VOC	Average
\mathcal{N} /LEEP [24]	-0.029	0.631	0.358	0.074	0.276	0.641	0.585	0.544	0.836	0.735	-0.076	0.416
LogME [44]	0.223	0.387	0.387	0.295	-0.028	0.627	0.718	0.570	0.704	0.217	0.121	0.384
GBC [30]	0.070	0.417	0.464	-0.054	0.237	0.317	0.701	0.729	0.484	0.539	0.161	0.370
SFDA [34]	0.254	0.526	0.553	0.619	0.548	0.815	0.847	0.685	0.556	0.732	0.532	0.606
NCTI [40]	0.035	0.643	0.724	0.546	0.533	0.715	0.705	0.892	0.767	0.697	0.547	0.619
LDA	0.058	0.708	0.720	0.707	0.692	0.913	0.779	0.944	0.540	0.892	0.723	0.698

Table 5. Performance comparison (average weighted Kendall τ_w) for LFT on self-supervised models. The highest performing τ_w value in each column are highlighted in bold. LDA achieves the highest overall average weighted Kendall τ_w score.

Method	Aircraft	Caltech-101	Cars	CIFAR10	CIFAR100	DTD	Flowers	Food-101	Pets	Sun397	VOC	Average
\mathcal{N} /LEEP [24]	0.446	0.654	0.537	-0.044	0.210	0.668	0.633	0.519	0.608	0.275	0.126	0.421
LogME [44]	0.569	0.350	0.629	-0.083	-0.250	0.655	0.653	0.518	0.487	-0.178	0.037	0.308
GBC [30]	0.498	0.446	0.717	-0.093	0.147	0.504	0.702	0.590	0.422	0.219	0.320	0.407
SFDA [34]	0.685	0.582	0.813	0.275	0.138	0.717	0.705	0.693	0.681	0.426	0.633	0.577
NCTI [40]	0.842	0.661	0.917	0.275	0.473	0.699	0.683	0.846	0.846	0.308	0.670	0.656
LDA	0.903	0.764	0.800	0.598	0.497	0.807	0.845	0.867	0.748	0.656	0.823	0.755

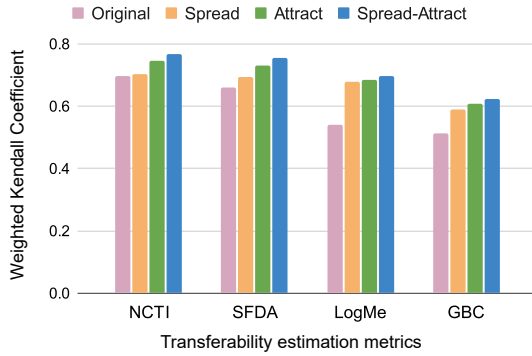


Figure 4. This figure demonstrates a bar chart that illustrates the performance improvement of various operations of feature perturbation over the original baseline. Each metric is represented by four bars, corresponding to different operations: Original, Spread, Attract, and Combined Spread-Attract, illustrating that the combined approach significantly outperform others.

of the entire feature space, maintaining a delicate balance between disrupting and preserving the structural integrity essential for accurate class differentiation. Moreover, the most substantial enhancement is observed when both operations are applied sequentially: first applying the Spread operation followed by the Attract operation. This sequential application leads to an average improvement of 17.82% over the originally obtained weighted Kendall coefficient. This demonstrates that the synergistic effect of applying both operations sequentially is significantly greater than the impact of each operation when applied independently.

4.4. Hyper-parameter Sensitivity Analysis

In this section, we assess the impact of key hyperparameters, namely σ and α , which govern the magnitude

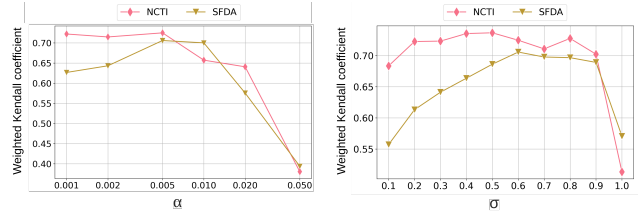


Figure 5. Hyper-parameter sensitivity analysis: The left figure showcases consistent performance (τ_w) across a wide range of α values, at optimum σ . This observation indicates an insensitivity to hyper-parameter changes. On the other hand, the right figure illustrates limited variance in performance (τ_w) across a broad spectrum of σ values, ranging from 0.5 to 0.9, at optimum α .

of perturbation within our method. The sensitivity analysis is conducted on two best-performed transferability estimation metrics (*i.e.*, SFDA and NCTI) after applying the proposed SA feature perturbation technique. Fig. 5 shows the ranking correlation under different σ and α . The minimal variations in performance across a wide range of hyper-parameters highlight the algorithm’s resilience, showcasing its robustness and reliability. We note that we fix the value of one hyper-parameter to tune the other one. From the figure, we can see that a similar performance trend is presented for both metrics. Specifically, the optimal performance is achieved at $\alpha = 0.005$ and $\sigma = 0.6$ for metrics. The analysis results demonstrate that the recommended hyper-parameters are versatile.

4.5. Time Complexity

Our feature perturbation strategy improves ranking correlation while maintaining the same level of time complexity, as shown in Fig. 6. The impact of our feature perturbation method on the time complexity of various transferabil-

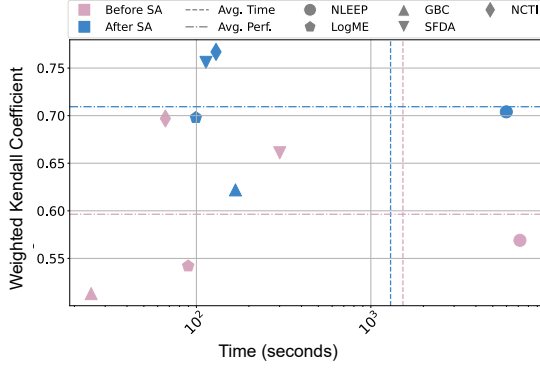


Figure 6. This figure compare the time complexity before and after applying feature perturbation techniques to vanilla fine-tuning.

ity estimation metrics has yielded mixed outcomes. While some metrics have experienced a reduction in time complexity, others have seen an increase, reflecting the effect of our feature perturbation method on different evaluation approaches. Metrics that rely heavily on the dimensionality of features such as \mathcal{N} LEEP, benefit from our method’s dimensionality reduction, which reduces processing time. However, metrics that are less dependent on feature dimensionality do not experience the same reductions in time complexity. In fact, the introduction of SA perturbation adds computational steps, slightly increasing overall time requirements.

4.6. Performance on Self-supervised Models

To evaluate the transferability estimation on the self-supervised models, we construct the pool with ResNet50 [15] pretrained on various self-supervised methods, spanning BYOL [13], Infomin [38], PCL-v1 [22], PCL-v2 [22], Sela-v2 [1], InsDis [42], SimCLR-v1 [7], SimCLR-v2 [8], MoCo-v1 [14], MoCo-v2 [9], DeepCluster-v2 [5], and SWAV [6]. In self-supervised tasks, we develop a baseline method, which leverages LDA to predict class probabilities for each sample and accumulate the probability of the correct class corresponding to samples as the transferability score. Further details can be found in supplementary material.

LDA-based metric achieves impressive results on transferability estimation of self-supervised models as shown in Table. 4 and Table. 5. For both vanilla fine-tuning (Table. 4) and LFT (Table. 5), LDA-based metric demonstrates a 12.7% and 15.06% higher average weighted Kendall coefficient compared to the best performing SOTA. The superior performance of the LDA-based metric compared to SOTA metrics across all fine-tuning types emphasizes a key insight: previous metrics have been primarily designed with supervised models in mind, overlooking the unique characteristics and requirements of self-supervised models. To understand why the LDA-based metric can outperform SOTA on self-supervised estimation tasks, we study the difference

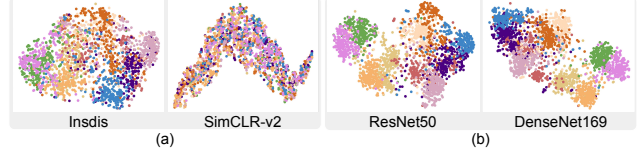


Figure 7. Comparison of CIFAR-10 embedding structures: (a) illustrates the embedding structure derived from a self-supervised model, while (b) depicts the embedding structure from a supervised model. Self-supervised models, learning without explicit label guidance, tend to capture more abstract relationships in the data, leading to embeddings with diverse patterns. In contrast, supervised models emphasize class separation, leading to a similar embedding structure for different models.

in feature geometry generated by the self-supervised and supervised models. The t-SNE feature visualization can be found in Fig. 7. Without semantic supervision, the self-supervised models present a more heterogeneous feature space than that of the supervised models. This finding also indicates that when estimating the transferability of models with diverse, less discriminative feature space, the existing transferability estimation metric could be vulnerable. On the other hand, the capability of the LDA metric to reflect the transferability of less discriminative feature spaces demonstrates a foundation for developing transferability estimation matrices for self-supervised models.

5. Conclusions and Discussions

The introduction and evaluation of our feature perturbation method represent a significant advancement in the field of transferability estimation. Through a comprehensive analysis, we have observed that our feature perturbation method not only enhances the accuracy of existing transferability metrics across various fine-tuning methods but also introduces a vital aspect of robustness evaluation. This additional layer of analysis provides more precise rankings by assessing the resilience of model embeddings to perturbations, ensuring that the best model is robust and transferable to new, target datasets. Specifically, our method has shown to significantly improve metrics such as \mathcal{N} LEEP, LogMe, GBC, SFDA, and NCTI with varied effects on time complexity, indicating its capacity to optimize computational efficiency in certain scenarios.

We provide insights into the disparities in embedding structures between self-supervised and supervised models, emphasizing the need for carefully tailored transferability estimation metrics for both model types. Our results reveal that an LDA-based metric outperforms SOTA across all fine-tuning variants for self-supervised tasks. This highlights an opportunity for the community to develop more adaptable and accurate transferability estimation metrics.

Acknowledgment

This work was supported in part by the Australian Research Council (FT230100426).

References

- [1] Yuki Markus Asano, Christian Rupprecht, and Andrea Vedaldi. Self-labelling via simultaneous clustering and representation learning. *arXiv preprint arXiv:1911.05371*, 2019. 8
- [2] Suresh Balakrishnama and Aravind Ganapathiraju. Linear discriminant analysis—a brief tutorial. *Institute for Signal and information Processing*, 18(1998):1–8, 1998. 2
- [3] Yoshua Bengio, Aaron Courville, and Pascal Vincent. Representation learning: A review and new perspectives. *IEEE transactions on pattern analysis and machine intelligence*, 35(8):1798–1828, 2013. 3
- [4] Lukas Bossard, Matthieu Guillaumin, and Luc Van Gool. Food-101—mining discriminative components with random forests. In *Computer Vision—ECCV 2014: 13th European Conference, Zurich, Switzerland, September 6–12, 2014, Proceedings, Part VI 13*, pages 446–461. Springer, 2014. 4
- [5] Mathilde Caron, Piotr Bojanowski, Armand Joulin, and Matthijs Douze. Deep clustering for unsupervised learning of visual features. In *ECCV*, pages 132–149, 2018. 8
- [6] Mathilde Caron, Ishan Misra, Julien Mairal, Priya Goyal, Piotr Bojanowski, and Armand Joulin. Unsupervised learning of visual features by contrasting cluster assignments. *NeurIPS*, 33:9912–9924, 2020. 8
- [7] Ting Chen, Simon Kornblith, Mohammad Norouzi, and Geoffrey Hinton. A simple framework for contrastive learning of visual representations. In *ICML*, 2020. 8
- [8] Ting Chen, Simon Kornblith, Kevin Swersky, Mohammad Norouzi, and Geoffrey E Hinton. Big self-supervised models are strong semi-supervised learners. *NeurIPS*, pages 22243–22255, 2020. 8
- [9] Xinlei Chen, Haoqi Fan, Ross Girshick, and Kaiming He. Improved baselines with momentum contrastive learning. *arXiv preprint arXiv:2003.04297*, 2020. 8
- [10] Mircea Cimpoi, Subhransu Maji, Iasonas Kokkinos, Sammy Mohamed, and Andrea Vedaldi. Describing textures in the wild. In *Proceedings of the IEEE conference on computer vision and pattern recognition*, pages 3606–3613, 2014. 5
- [11] M. Everingham, L. Van Gool, C. K. I. Williams, J. Winn, and A. Zisserman. The PASCAL Visual Object Classes Challenge 2007 (VOC2007) Results. <http://www.pascal-network.org/challenges/VOC/voc2007/workshop/index.html>. 5
- [12] Li Fei-Fei. Learning generative visual models from few training examples. In *Workshop on Generative-Model Based Vision, IEEE Proc. CVPR, 2004*, 2004. 5
- [13] Jean-Bastien Grill, Florian Strub, Florent Altché, Corentin Tallec, Pierre Richemond, Elena Buchatskaya, Carl Doersch, Bernardo Avila Pires, Zhaohan Guo, Mohammad Gheshlaghi Azar, et al. Bootstrap your own latent—a new approach to self-supervised learning. *NeurIPS*, pages 21271–21284, 2020. 8
- [14] Kaiming He, Haoqi Fan, Yuxin Wu, Saining Xie, and Ross Girshick. Momentum contrast for unsupervised visual representation learning. In *CVPR*, pages 9729–9738, 2020. 8
- [15] Kaiming He, Xiangyu Zhang, Shaoqing Ren, and Jian Sun. Deep residual learning for image recognition. In *2016 IEEE Conference on Computer Vision and Pattern Recognition, CVPR 2016, Las Vegas, NV, USA, June 27–30, 2016*, pages 770–778. IEEE Computer Society, 2016. 5, 8
- [16] Gao Huang, Zhuang Liu, Laurens van der Maaten, and Kilian Q. Weinberger. Densely connected convolutional networks. In *2017 IEEE Conference on Computer Vision and Pattern Recognition, CVPR 2017, Honolulu, HI, USA, July 21–26, 2017*, pages 2261–2269. IEEE Computer Society, 2017. 5
- [17] Maurice G Kendall. A new measure of rank correlation. *Biometrika*, 30(1/2):81–93, 1938. 5
- [18] Polina Kirichenko, Pavel Izmailov, and Andrew Gordon Wilson. Last layer re-training is sufficient for robustness to spurious correlations. *arXiv preprint arXiv:2204.02937*, 2022. 2
- [19] Jonathan Krause, Jia Deng, Michael Stark, and Li Fei-Fei. Collecting a large-scale dataset of fine-grained cars. 2013. 4
- [20] Alex Krizhevsky, Geoffrey Hinton, et al. Learning multiple layers of features from tiny images. 2009. 5
- [21] Ananya Kumar, Aditi Raghunathan, Robbie Jones, Tengyu Ma, and Percy Liang. Fine-tuning can distort pretrained features and underperform out-of-distribution. *arXiv preprint arXiv:2202.10054*, 2022. 2
- [22] Junnan Li, Pan Zhou, Caiming Xiong, and Steven CH Hoi. Prototypical contrastive learning of unsupervised representations. *arXiv preprint arXiv:2005.04966*, 2020. 8
- [23] Xiaotong Li, Zixuan Hu, Yixiao Ge, Ying Shan, and Lingyu Duan. Exploring model transferability through the lens of potential energy. In *Proceedings of the IEEE/CVF International Conference on Computer Vision*, pages 5429–5438, 2023. 3
- [24] Yihao Li, Xiaogang Jia, Rongjie Sang, Yi Zhu, Bryan Green, Le Song, and Boqing Gong. Ranking neural checkpoints. In *Proceedings of the IEEE/CVF Conference on Computer Vision and Pattern Recognition (CVPR)*, pages 2663–2673, 2021. 1, 2, 3, 5, 6, 7
- [25] Subhransu Maji, Esa Rahtu, Juho Kannala, Matthew Blaschko, and Andrea Vedaldi. Fine-grained visual classification of aircraft. *arXiv preprint arXiv:1306.5151*, 2013. 4
- [26] Tarun Ram Menta, Surgan Jandial, Akash Patil, Saketh Bachu, Vimal KB, Balaji Krishnamurthy, Vineeth N Balasubramanian, Mausoom Sarkar, and Chirag Agarwal. Active transferability estimation. In *Proceedings of the IEEE/CVF Conference on Computer Vision and Pattern Recognition*, pages 2659–2670, 2024. 3
- [27] Sebastian Mika, Gunnar Ratsch, Jason Weston, Bernhard Scholkopf, and Klaus-Robert Mullers. Fisher discriminant analysis with kernels. In *Neural networks for signal processing IX: Proceedings of the 1999 IEEE signal processing society workshop (cat. no. 98th8468)*, pages 41–48. Ieee, 1999. 3

- [28] Cuong V. Nguyen, Tal Hassner, Matthias Seeger, and Cedric Archambeau. Leep: A new measure to evaluate transferability of learned representations. *Proceedings of the 37th International Conference on Machine Learning (ICML 2020)*, 119:7479–7489, 2020. 1, 2
- [29] Maria-Elena Nilsback and Andrew Zisserman. Automated flower classification over a large number of classes. In *2008 Sixth Indian conference on computer vision, graphics & image processing*, pages 722–729. IEEE, 2008. 4
- [30] Michal Pandý, Andrea Agostinelli, Jasper Uijlings, Vittorio Ferrari, and Thomas Mensink. Transferability estimation using bhattacharyya class separability. In *Proceedings of the IEEE/CVF Conference on Computer Vision and Pattern Recognition*, pages 9172–9182, 2022. 1, 2, 3, 5, 6, 7
- [31] Omkar M Parkhi, Andrea Vedaldi, Andrew Zisserman, and CV Jawahar. Cats and dogs. In *2012 IEEE conference on computer vision and pattern recognition*, pages 3498–3505. IEEE, 2012. 4
- [32] Douglas A Reynolds et al. Gaussian mixture models. *Encyclopedia of biometrics*, 741(659-663), 2009. 3
- [33] Mark Sandler, Andrew G. Howard, Menglong Zhu, Andrey Zhmoginov, and Liang-Chieh Chen. Mobilenetv2: Inverted residuals and linear bottlenecks. In *2018 IEEE Conference on Computer Vision and Pattern Recognition, CVPR 2018, Salt Lake City, UT, USA, June 18-22, 2018*, pages 4510–4520. Computer Vision Foundation / IEEE Computer Society, 2018. 5
- [34] Wenqi Shao, Xun Zhao, Yixiao Ge, Zhaoyang Zhang, Lei Yang, Xiaogang Wang, Ying Shan, and Ping Luo. Not all models are equal: predicting model transferability in a self-challenging fisher space. In *European Conference on Computer Vision*, pages 286–302. Springer, 2022. 1, 2, 3, 4, 5, 6, 7
- [35] Christian Szegedy, Wei Liu, Yangqing Jia, Pierre Sermanet, Scott E. Reed, Dragomir Anguelov, Dumitru Erhan, Vincent Vanhoucke, and Andrew Rabinovich. Going deeper with convolutions. In *IEEE Conference on Computer Vision and Pattern Recognition, CVPR 2015, Boston, MA, USA, June 7-12, 2015*, pages 1–9. IEEE Computer Society, 2015. 5
- [36] Christian Szegedy, Vincent Vanhoucke, Sergey Ioffe, Jonathon Shlens, and Zbigniew Wojna. Rethinking the inception architecture for computer vision. In *2016 IEEE Conference on Computer Vision and Pattern Recognition, CVPR 2016, Las Vegas, NV, USA, June 27-30, 2016*, pages 2818–2826. IEEE Computer Society, 2016. 5
- [37] Mingxing Tan, Bo Chen, Ruoming Pang, Vijay Vasudevan, Mark Sandler, Andrew Howard, and Quoc V. Le. Mnasnet: Platform-aware neural architecture search for mobile. In *IEEE Conference on Computer Vision and Pattern Recognition, CVPR 2019, Long Beach, CA, USA, June 16-20, 2019*, pages 2820–2828. Computer Vision Foundation / IEEE, 2019. 5
- [38] Yonglong Tian, Chen Sun, Ben Poole, Dilip Krishnan, Cordelia Schmid, and Phillip Isola. What makes for good views for contrastive learning? *NeurIPS*, 33:6827–6839, 2020. 8
- [39] Anh T. Tran, Cuong V. Nguyen, and Tal Hassner. Transferability and hardness of supervised classification tasks. In *Proceedings of the IEEE/CVF International Conference on Computer Vision (ICCV)*, pages 1395–1405, 2019. 1, 2
- [40] Zijian Wang, Yadan Luo, Liang Zheng, Zi Huang, and Mahsa Baktashmotlagh. How far pre-trained models are from neural collapse on the target dataset informs their transferability. In *IEEE/CVF International Conference on Computer Vision, ICCV 2023, Paris, France, October 1-6, 2023*, pages 5526–5535. IEEE, 2023. 1, 2, 3, 5, 6, 7
- [41] Svante Wold, Kim Esbensen, and Paul Geladi. Principal component analysis. *Chemometrics and intelligent laboratory systems*, 2(1-3):37–52, 1987. 3
- [42] Zhirong Wu, Yuanjun Xiong, Stella X Yu, and Dahua Lin. Unsupervised feature learning via non-parametric instance discrimination. In *CVPR*, pages 3733–3742, 2018. 8
- [43] Jianxiong Xiao, James Hays, Krista A Ehinger, Aude Oliva, and Antonio Torralba. Sun database: Large-scale scene recognition from abbey to zoo. In *2010 IEEE computer society conference on computer vision and pattern recognition*, pages 3485–3492. IEEE, 2010. 5
- [44] Kun You, Yinhan Liu, Jianbo Wang, and Minglong Long. Logme: Practical assessment of pre-trained models for transfer learning. In *Proceedings of the 38th International Conference on Machine Learning (ICML)*, page 12133–12143. PMLR, 2021. 1, 2, 3, 5, 6, 7
- [45] Yi-Kai Zhang, Ting-Ji Huang, Yao-Xiang Ding, De-Chuan Zhan, and Han-Jia Ye. Model spider: Learning to rank pre-trained models efficiently. *Advances in Neural Information Processing Systems*, 36, 2024. 1
- [46] Fuzhen Zhuang, Zhiyuan Qi, Keyu Duan, Dongbo Xi, Yongchun Zhu, Hengshu Zhu, Hui Xiong, and Qing He. A comprehensive survey on transfer learning. *Proceedings of the IEEE*, 109(1):43–76, 2020. 1

Supplementary Material

The supplementary material contains additional details and further results related to the main paper.

A. Implementation details of LDA-Based Score

This section describes the implementation process for deriving a classification score based on Linear Discriminant Analysis (LDA). LDA finds a linear combination of features that best separate the classes of data. The core optimization problem of LDA is expressed as:

$$U = \arg \max_U \frac{U^T \Sigma_\beta U}{U^T \Sigma_\omega U}, \quad (6)$$

where Σ_β and Σ_ω represent the between-class and within-class scatter matrices, respectively. This formula aims to project feature vectors to maximize the ratio of between-class variance to within-class variance.

To solve this optimization, we follow the methodology outlined in Ghojogh et al. (2019), which leads to the solution of the generalized eigenvalue problem:

$$U = \text{eig}((\Sigma_\omega + \epsilon I)^{-1} \Sigma_\beta), \quad (7)$$

where ϵ is a small positive scalar that ensures the non-singularity of the within-class scatter matrix Σ_ω .

In our transformed feature space, each class's features are assumed to follow a normal distribution centered at their projected class means. Bayes' theorem expresses the score function for a sample for label c as in Eq. 9. We then compute the LDA-based metric score S_{lda} using:

$$\bar{f} = U^T \mathcal{F}, \quad (8)$$

$$\delta_c = \bar{f}^T U^T \mu_c - \frac{1}{2} \mu_c^T U U^T \mu_c + \log\left(\frac{K_c}{K}\right), \quad (9)$$

$$S_{lda} = \frac{1}{K} \sum_{k=1}^K \frac{e^{\delta_y}}{\sum_{c=1}^C e^{\delta_c}}, \quad (10)$$

where y is the ground-truth class label, K is the total number of samples, and C is the number of classes. The S_{lda} represents the probability of correctly classifying a sample based on the calculated discriminative scores δ_c for each class.

B. More experimental results

This section presents experimental results that were not included in the main paper due to space limitations.

B.1. LBFT for self-supervised models

Besides vanilla fine-tuning and LFT for self-supervised models, LDA-based metrics also demonstrate improved

performance in transferability estimation for LBFT. (see Table 6). The overall average values of these metrics are significantly lower compared to LFT and vanilla fine-tuning. This indicates that the previous metrics are not well-suited for LBFT fine-tuning. Observing Table 8, it's evident that the Aircraft dataset exhibits the lowest target accuracy among all datasets, suggesting that self-supervised models pre-trained with ImageNet may not be optimally suited for transfer to the Aircraft dataset. This influence is further highlighted in Table 6, where the performance of all previous metrics for the Aircraft dataset shows negative correlation scores, showing that the metric may not rank the model properly based on the feature embedding.

C. Visualization: Correlation between the metric and accuracy

Fig. 8 depicts the relationship between the ground truth target accuracy (vanilla fine-tuning) and the transferability estimation metric score across various datasets. We use the best two metrics (*i.e.*, SFDA and NCTI) to illustrate the regression plots for the original metric (depicted in pink) following the application of our feature perturbation method (depicted in blue). The shaded area indicates the 95 confidence interval. After applying our feature perturbation, the width of the shaded region in the regression plot decreases, indicating the metric score and target accuracy are more linearly correlated. Additionally, the ranking of many models shifts, bringing them closer to the shaded area, resulting in an enhancement in the weighted Kendall τ_w .

D. Downstream datasets description

We validate the effectiveness of the proposed methods on 11 standard datasets commonly adopted in transferability estimation metric evaluation. The datasets can be categorized as follows:

1. Fine-grained classification datasets:

- **FGVC Aircraft:** This dataset contains images of various aircraft types for fine-grained classification. It consists of 100 classes with a total of 10,000 images, split into a 2:3 ratio for training and testing.
- **Stanford Cars:** Comprising images of cars from different viewpoints, this dataset totals 16,185 images across various car brands and models, providing a diverse set of images for training and evaluation. The training set contains 8,144 images, while the test set contains 8,041 images.
- **Food-101:** A dataset with 101,000 images categorized into 101 food classes. Each food cate-

gory contains 750 training images and 250 testing images.

- Oxford-IIIT Pets: This dataset includes 7,049 pet images belonging to 37 different pet breeds with a varying number of images per breed. The training set consists of 3,680 images, and the testing set has 3,669 images.
- Oxford-102 Flowers: It has 102 categories with varying numbers of images per category. It comprises between 40 and 258 images per category, with 20 images sampled for training and the remaining 6,149 images for testing.

2. Coarse-grained classification dataset:

- Caltech-101: A dataset with 9,146 images distributed among 101 categories. 70% of the data is sampled for the training set.
- CIFAR-10 and CIFAR-100: These datasets contain 60,000 color images of object categories, including animals, vehicles, and everyday objects, making them suitable for general-purpose image classification. CIFAR-10 is divided into 10 distinct classes with 5,000 training images and 1,000 testing images per class. CIFAR-100 is divided into 100 distinct classes with 500 training images and 100 testing images per class.
- VOC2007: This dataset consists of 9,963 images across 20 classes with a variety of common object classes, including people, animals, vehicles, and household items. The training set comprises 5,011 images and the remaining for testing.

3. Scene classification dataset:

- SUN397: This dataset contains 397 classes, each with 1,000 scenery pictures, totaling 19,850 images. The dataset covers a wide range of scenes, including indoor/outdoor environments, and natural/urban settings.

4. Texture classification dataset:

- DTD: This dataset includes 5,640 textural images categorized into 47 classes. The dataset includes high-quality images with variations in lighting, scale, and orientation, making it suitable for studying the challenges of texture recognition in real-world scenarios. Each class contains 80 training images and 40 testing images.

E. Ground Truth

The ground truth target accuracies of vanilla FT, LBFT, and LFT for supervised models are given in Table. 7, 8, 9. For self-supervised models, the ground truth target accuracies are given in Table. 10, 11, 12. For both LBFT and LFT, we follow the grid search described in [34], which selects the learning rates from $\{10^{-1}, 10^{-2}, 10^{-3}, 10^{-4}\}$ and weight decay parameters from $\{10^{-6}, 10^{-5}, 10^{-4}, 10^{-3}\}$. Once the optimal hyper-parameters are identified, we proceed to fine-tune the pre-trained model on the designated dataset using these hyper-parameters. The resulting test accuracy serves as our benchmark. Fine-tuning is conducted on a NVIDIA A100, utilizing a batch size of 128, and all input images are resized to dimensions of 224×224. To ensure the robustness and reliability of our evaluation, we execute the code using five distinct seeds for each experiment.

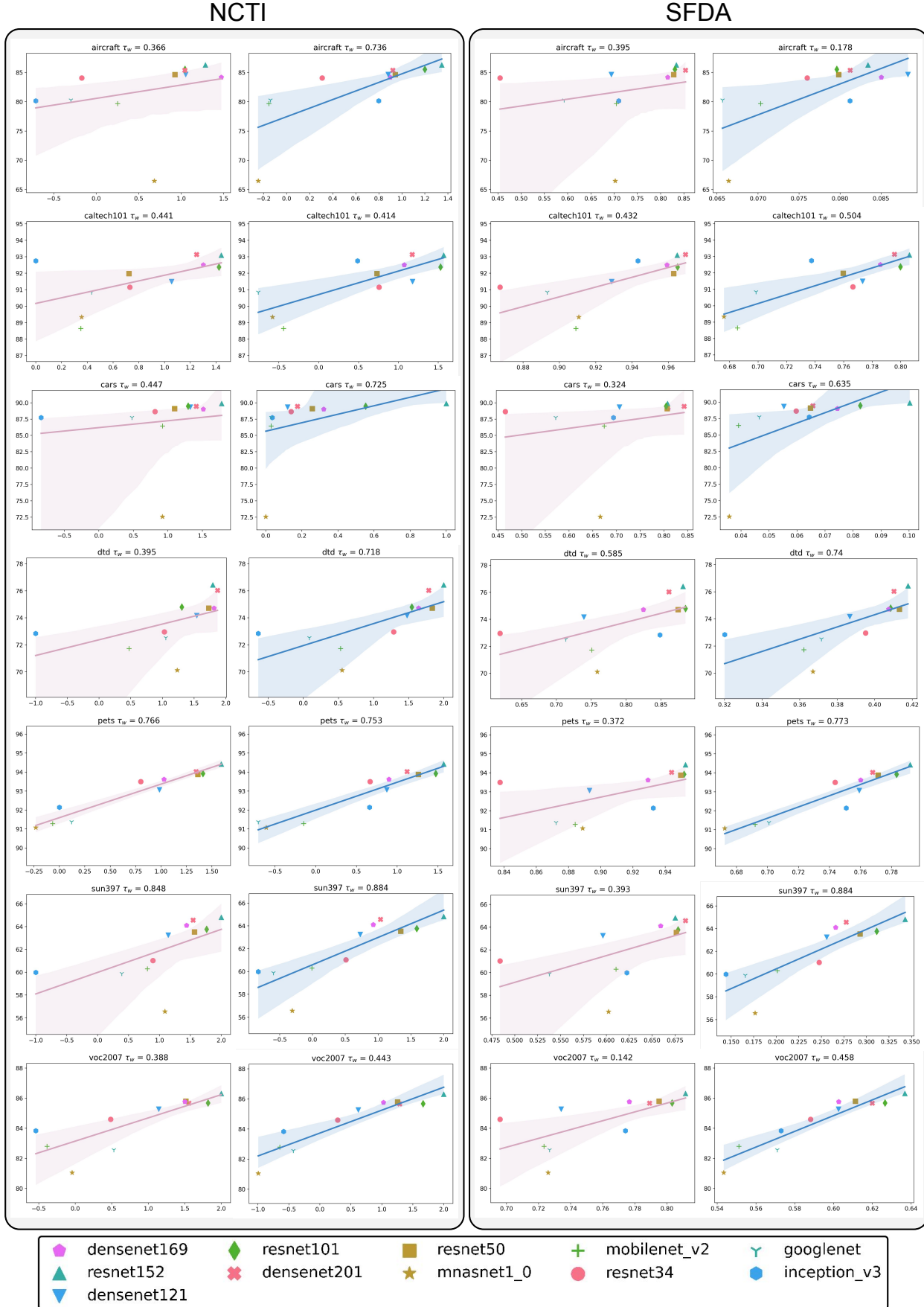


Figure 8. The figure illustrates the correlation between transferability scores and model performance (%) on the target dataset after vanilla fine-tuning (best viewed in color). Each marker denotes a distinct supervised pre-trained model. We demonstrate an enhancement for NCTI and SFDA using the weighted Kendall τ_w of our feature perturbation method (in blue) over the original method (in pink).

Table 6. Performance comparison (average weighted Kendall τ_w) for LBFT on self-supervised models. The highest performing τ_w value in each column are highlighted in bold. LDA achieves the highest overall average weighted Kendall τ_w score.

Method	Aircraft	Caltech-101	Cars	CIFAR10	CIFAR100	DTD	Flowers	Food-101	Pets	Sun397	VOC	Average
\mathcal{N} LEEP [24]	-0.288	0.600	0.277	0.291	0.326	0.849	0.283	0.603	0.683	0.099	0.184	0.355
LogME [43]	-0.117	0.326	0.237	-0.177	-0.183	0.836	0.512	0.645	0.708	-0.157	0.407	0.276
GBC [29]	-0.244	0.342	0.171	0.263	0.264	0.472	0.417	0.495	0.485	0.247	0.408	0.302
SFDA [33]	-0.189	0.465	0.088	-0.056	0.056	0.707	0.357	0.550	0.738	0.163	0.688	0.324
NCTI [39]	-0.194	0.610	0.046	-0.077	0.428	0.895	0.372	0.421	0.757	0.256	0.738	0.387
LDA	-0.282	0.655	0.720	0.169	0.330	0.686	0.353	0.462	0.670	0.588	0.681	0.389

Table 7. The ground truth target accuracy of vanilla fine-tuning for supervised models on 11 target datasets is sourced from [33].

	Aircraft	Caltech-101	Cars	CIFAR10	CIFAR100	DTD	Flowers	Food-101	Pets	Sun	VOC
ResNet-34	84.06	91.15	88.63	96.12	81.94	72.96	95.2	81.99	93.5	61.02	84.6
ResNet-50	84.64	91.98	89.09	96.28	82.8	74.72	96.26	84.45	93.88	63.54	85.8
ResNet-101	85.53	92.38	89.47	97.39	84.88	74.8	96.53	85.58	93.92	63.76	85.68
ResNet-152	86.29	93.1	89.88	97.53	85.66	76.44	96.86	86.28	94.42	64.82	86.32
DenseNet-121	84.66	91.5	89.34	96.45	82.75	74.18	97.02	84.99	93.07	63.26	85.28
DenseNet-169	84.19	92.51	89.02	96.77	84.26	74.72	97.32	85.84	93.62	64.1	85.77
DenseNet-201	85.38	93.14	89.44	97.02	84.88	76.04	97.1	86.71	94.03	64.57	85.67
MNet-A1	66.48	89.34	72.58	92.59	72.04	70.12	95.39	71.35	91.08	56.56	81.06
MobileNetV2	79.68	88.64	86.44	94.74	78.11	71.72	96.2	81.12	91.28	60.29	82.8
Googlenet	80.32	90.85	87.76	95.54	79.84	72.53	95.76	79.3	91.38	59.89	82.58
InceptionV3	80.15	92.75	87.74	96.18	81.49	72.85	95.73	81.76	92.14	59.98	83.84

Table 8. The ground truth target accuracy of LBFT for supervised models on 11 target datasets.

	Aircraft	Caltech-101	Cars	CIFAR10	CIFAR100	DTD	Flowers	Food-101	Pets	Sun	VOC
InceptionV3	47.98	90.25	56.6	83.76	63.46	68.99	90.76	63.77	87.78	81.6	80.88
MobileNetV2	53.33	86.78	69.83	87.06	66.59	73.19	94.95	72.24	90.41	83.26	82.03
MNet-A1	52.05	88.92	65.08	74.4	40.68	68.03	93.95	67.05	90.54	73	82.37
DenseNet-121	67.81	90.24	81.72	93.7	78.23	72.93	97.36	79.29	91.26	90.39	84.42
DenseNet-169	74.29	92.51	83.94	96.06	84.2	74.36	96.47	82.06	93.65	96.83	86.03
DenseNet-201	71.51	92.02	83.51	95.74	83.85	74.41	97.36	81.94	91.89	97.02	85.36
ResNet-34	70.94	90.42	83.07	93.94	80.74	71.54	96.42	78.04	92.84	94.84	84.39
ResNet-50	76.43	91.4	84.93	86.49	84.46	74.57	97.25	82.8	93.87	96.28	85.67
ResNet-101	75.57	91.92	85.19	96.34	85.04	74.79	96.48	83.02	93.44	97.41	85.76
ResNet-152	74.68	92.45	85.75	96.18	84.73	75.16	95.41	82.86	93.93	96.56	86.15
Googlenet	64.55	90.31	78.06	92.67	76.1	72.82	95.08	72.69	89.67	92.4	80.75

Table 9. The ground truth target accuracy of LFT for supervised models on 11 target datasets.

	Aircraft	Caltech-101	Cars	CIFAR10	CIFAR100	DTD	Flowers	Food-101	Pets	Sun	VOC
InceptionV3	28.21	88.48	27.6	69.87	46.39	61.28	83.01	46.31	85.85	63.72	77.01
MobileNetV2	42.24	87.35	49.77	76.97	57.46	67.77	92.27	62.6	89.73	73.25	80.88
MNet-A1	41.72	87.85	46.19	69.55	37.49	65.69	92.37	62.65	89.56	79.63	81.18
DenseNet-121	43.61	90.03	51.78	81.39	62.11	68.09	93.23	65.37	91.46	76.37	82.73
DenseNet-169	47.15	90.76	56.2	83.08	64.53	69.95	94.15	67.81	92.6	80.78	84.07
DenseNet-201	46.39	91.31	57.32	84.52	67.51	70.64	93.01	68.11	92.57	80.38	83.34
ResNet-34	38.19	89.8	32.04	78.61	59.43	66.7	90.71	60.56	91.27	71.96	82.46
ResNet-50	40.63	89.75	50.91	83.57	65.41	70.74	93.05	65.79	91.76	83.29	83.28
ResNet-101	41.21	89.81	50.6	85.24	67.64	69.57	92.3	66.5	92.34	75.61	83.85
ResNet-152	42.98	91.42	52.07	85.33	67.81	70.74	93.06	67.55	92.67	75.72	84.13
Googlenet	36.22	88.31	43.83	78.45	59.73	66.12	89.53	55.34	89.41	76.82	80.32

Table 10. The ground truth target accuracy of vanilla fine-tuning for self-supervised models on 11 target datasets is sourced from [33].

	Aircraft	Caltech-101	Cars	CIFAR10	CIFAR100	DTD	Flowers	Food-101	Pets	Sun	VOC
BYOL	82.10	91.90	89.83	96.98	83.86	76.37	96.80	85.44	91.48	63.69	85.13
Deepclusterv2	82.43	91.16	90.16	97.17	84.84	77.31	97.05	87.24	90.89	66.54	85.38
Infomin	83.78	80.86	86.90	96.72	70.89	73.47	95.81	78.82	90.92	57.67	81.41
InsDis	79.70	77.21	80.21	93.08	69.08	66.40	93.63	76.47	84.58	51.62	76.33
MoCov1	81.85	79.68	82.19	94.15	71.23	67.36	94.32	77.21	85.26	53.83	77.94
MoCov2	83.70	82.76	85.55	96.48	71.27	72.56	95.12	77.15	89.06	56.28	78.32
PCLv1	82.16	88.60	87.15	96.42	79.44	73.28	95.62	77.70	88.93	58.36	81.91
PCLv2	83.00	87.52	85.56	96.55	79.84	69.3	95.87	80.29	88.72	58.82	81.85
Sela-v2	85.42	90.53	89.85	96.85	84.36	76.03	96.22	86.37	89.61	65.74	85.52
SimCLRv1	80.54	90.94	89.98	97.09	84.49	73.97	95.33	82.2	88.53	63.46	83.29
SimCLRv2	81.50	88.58	88.82	96.22	78.91	74.71	95.39	82.23	89.18	60.93	83.08
SWAV	83.04	89.49	89.81	96.81	83.78	76.68	97.11	87.22	90.59	66.10	85.06

Table 11. The ground truth target accuracy of LBFT for self-supervised models on 11 target datasets.

	Aircraft	Caltech-101	Cars	CIFAR10	CIFAR100	DTD	Flowers	Food-101	Pets	Sun	VOC
BYOL	73.09	91.05	85.15	98.50	92.52	74.68	96.16	83.11	89.60	99.81	84.06
Deepclusterv2	71.16	89.62	83.26	95.95	84.62	75.21	95.87	83.29	89.82	99.79	84.59
Infomin	77.46	84.77	85.57	96.31	82.15	74.63	96.18	84.25	88.60	98.62	82.56
InsDis	70.65	76.14	79.48	94.16	77.20	70.74	91.91	79.05	80.28	97.96	76.50
MoCov1	73.16	78.40	81.40	94.35	77.97	71.49	92.24	78.70	83.05	98.02	78.10
MoCov2	75.70	85.18	84.37	96.23	82.12	73.46	95.47	82.57	87.78	97.87	81.20
PCLv1	76.60	85.63	83.82	96.94	85.98	73.03	94.78	80.82	85.83	99.13	80.87
PCLv2	76.65	85.07	84.94	97.75	87.97	72.45	95.11	82.62	87.05	99.17	81.42
Sela-v2	69.85	87.56	81.66	95.56	83.75	74.36	94.94	82.62	88.54	99.53	85.19
SimCLRv1	67.45	90.48	77.08	96.96	87.65	71.65	92.13	75.77	85.43	99.48	82.29
SimCLRv2	74.04	85.19	84.83	97.38	89.90	72.45	95.50	83.09	84.92	99.85	80.76
SWAV	71.65	88.49	82.84	95.72	83.69	75.85	95.66	83.31	87.62	99.80	84.22

Table 12. The ground truth target accuracy of LFT for self-supervised models on 11 target datasets.

	Aircraft	Caltech-101	Cars	CIFAR10	CIFAR100	DTD	Flowers	Food-101	Pets	Sun	VOC
BYOL	43.48	89.83	43.45	84.07	57.71	71.28	92.75	61.17	87.13	66.36	74.79
Deepclusterv2	47.44	89.34	56.19	79.43	55.19	72.45	93.65	68.62	87.08	81.41	80.91
Infomin	12.81	80.61	7.24	58.89	22.09	65.11	63.58	37.98	80.96	38.14	74.28
InsDis	10.93	51.26	3.82	42.81	15.65	56.33	58	27.06	50.77	31.08	52.17
MoCov1	10.88	54.23	3.32	45.01	15.68	54.41	54.56	26.89	53.03	31.01	55.92
MoCov2	11.51	78.43	5.52	54.22	24.09	64.89	59.73	34.86	73.62	34.81	70.54
PCLv1	7.46	70.13	3.90	50.70	22.68	52.23	36.81	21.12	68.08	25.84	67.99
PCLv2	13.99	82.41	8.20	69.79	32.66	65.90	69.71	36.15	75.51	39.06	72.15
Sela-v2	31.31	84.62	24.40	73.00	38.91	72.07	87.64	58.06	82.27	65.42	77.46
SimCLRv1	42.75	88.72	43.23	83.77	61.60	67.07	88.42	58.55	79.86	82.51	78.87
SimCLRv2	39.96	86.66	42.54	80.74	55.51	71.97	91.34	63.24	81.79	76.51	77.76
SWAV	43.25	87.85	45.94	75.93	47.59	74.15	92.54	66.42	85.23	77.48	79.28